

RESEARCH ARTICLE

Conformational Dynamics of Response Regulator RegX3 from *Mycobacterium tuberculosis*

Ashfaq Ahmad¹, Yongfei Cai¹, Xingqiang Chen², Jianwei Shuai², Aidong Han^{1*}

1 State Key Laboratory for Cellular Stress Biology, School of Life Sciences, Xiamen University, Xiangan, Xiamen, China, **2** Department of Physics, Xiamen University, Siming, Xiamen, China

* ahan@xmu.edu.cn



OPEN ACCESS

Citation: Ahmad A, Cai Y, Chen X, Shuai J, Han A (2015) Conformational Dynamics of Response Regulator RegX3 from *Mycobacterium tuberculosis*. PLoS ONE 10(7): e0133389. doi:10.1371/journal.pone.0133389

Editor: Claudio M Soares, Instituto de Tecnológica Química e Biológica, UNL, PORTUGAL

Received: April 8, 2015

Accepted: June 25, 2015

Published: July 22, 2015

Copyright: © 2015 Ahmad et al. This is an open access article distributed under the terms of the [Creative Commons Attribution License](https://creativecommons.org/licenses/by/4.0/), which permits unrestricted use, distribution, and reproduction in any medium, provided the original author and source are credited.

Data Availability Statement: All relevant data are within the paper and its Supporting Information files.

Funding: This work was supported by National Science Foundation of China (31070647 and 31370723 to AH; 31370830 and 11125419 to JS), National Key Basic Research Program (2013CB910603 to AH.), Project 985 (2011121028 to AH). The funders had no role in study design, data collection and analysis, decision to publish, or preparation of the manuscript.

Competing Interests: The authors have declared no competing interest exist.

Abstract

Two-component signal transduction systems (TCS) are vital for adaptive responses to various environmental stresses in bacteria, fungi and even plants. A TCS typically comprises of a sensor histidine kinase (SK) with its cognate response regulator (RR), which often has two domains—N terminal receiver domain (RD) and C terminal effector domain (ED). The histidine kinase phosphorylates the RD to activate the ED by promoting dimerization. However, despite significant progress on structural studies, how RR transmits activation signal from RD to ED remains elusive. Here we analyzed active to inactive transition process of OmpR/PhoB family using an active conformation of RegX3 from *Mycobacterium tuberculosis* as a model system by computational approaches. An inactive state of RegX3 generated from 150 ns molecular dynamic simulation has rotameric conformations of Thr⁷⁹ and Tyr⁹⁸ that are generally conserved in inactive RRs. Arg⁸¹ in loop β4α4 acts synergistically with loop β1α1 to change its interaction partners during active to inactive transition, potentially leading to the N-terminal movement of RegX3 helix α1. Global conformational dynamics of RegX3 is mainly dependent on α4β5 region, in particular seven ‘hot-spot’ residues (Tyr⁹⁸ to Ser¹⁰⁴), adjacent to which several coevolved residues at dimeric interface, including Ile⁷⁶-Asp⁹⁶, Asp⁹⁷-Arg¹¹¹ and Glu²⁴-Arg¹¹³ pairs, are critical for signal transduction. Taken together, our computational analyses suggest a molecular linkage between Asp phosphorylation, proximal loops and α4β5α5 dimeric interface during RR active to inactive state transition, which is not often evidently defined from static crystal structures.

Introduction

Microorganisms have been evolved with many sophisticated signal transduction systems to rapidly respond to various kinds of external and/or internal stimuli. Two-component systems (TCSs) have emerged as a major signal transduction pathway in microorganisms [1]. A typical TCS contains a membrane-integrated sensor histidine kinase (SK) and a response regulator (RR). A SK, which senses and interprets stimuli to activate its cognate cytoplasmic RR through

phosphorylation, usually performs autokinase, phosphatase and phosphotransferase activities. RR mostly outputs as a transcription factor to alter expression level of specific set of genes [2, 3]. The phosphorylation is absolutely specific and conserved on a histidine residue in SK and an aspartic acid residue in RR, which is believed to initiate favorable conformational changes to promote RR dimer formation and stabilization [4, 5].

SenX3-RegX3 is an essential TCS for the survival and progressive infection of mycobacteria [6]. This TCS induces transcription of *phoA* and *pstS* genes in phosphate limiting environment [7] and also controls expression of several critical metabolic enzymes Ald, CydB and GltA1 in aerobic condition [8]. RegX3, which belongs to OmpR/PhoB family, comprises of two domains, N-terminal receiver domain (RD) and C-terminal effector domain (ED). The ED is a DNA-binding with a characteristic structure of winged helix-turn-helix (wHTH) and involved in transcriptional regulation upon phosphorylation of Asp⁵² in its RD [3, 9].

Structures of seven full-length OmpR/PhoB family members, MtrA, PrrA, DrrB, DrrD, PhoP, BaeR and RegX3 have been solved by X-ray crystallography [10–16]. All the structures, but not RegX3, are present in inactive state and therefore RegX3 becomes only a structure captured in active state, which is stabilized by five lanthanum ions used in crystallization condition. The La³⁺ ion that stabilizes the active site of RegX3 coordinates with Asp⁹ (β 1 α 1 loop), Asp⁵², Met⁵⁴ (β 3 α 3 loop) and Glu⁸⁴ (α 4) where Asp⁹ and Asp⁵² prevent the steric clash. Moreover the position of La³⁺ ion almost coincides with Mg²⁺ in PhoB (PDB ID: 1ZES) [13, 17]. In CheY RR, trivalent cations are shown to bind tightly than divalent cations and suggested the importance of high positive charge that could further neutralize the repulsive effect of the carboxylate amino acids in the active site [18]. The active RegX3 has a unique domain-swapped dimer interface of α 4 β 5 α 5 face in OmpR/PhoB family [17, 19]. The two signature switch residues Thr⁷⁹ and Tyr⁹⁸ form a so-called Y-T coupling or *gauche+* conformation, where Thr⁷⁹ OH group points to the conserved Asp⁵² [3, 13].

Macromolecular structures determined by X-ray crystallography can be possibly restricted or even changed in crystallization conditions [20]. Neither cryo-EM nor NMR is sufficient to provide a complete and dynamic picture of molecules. Molecular Dynamics (MD) is able to simulate a macromolecular structure in a relaxed and physiological condition, which provides significant insights on protein functions at molecular level [21, 22]. The diverse structures of the full-length RRs indicate that a RR is capable to reorient both the RD and ED in response to phosphorylation-induced activation [23]; however, a comprehensive analysis of critical residues has not been reported. Here we took co-evolution analysis for OmpR/PhoB family, which was further supported by MD and normal mode analysis (NMA) using RegX3 as a model. We observed several key conformational changes in the local flexible regions of RegX3 phosphorylation site in addition to critical proximal residues, revealing a plausible molecular mechanism that transmits global transition signals between RD and ED upon phosphorylation.

Results

Inactive state of RegX3

The full-length RegX3 structure was solved in active conformation stabilized by domain swapping [13]. To obtain an inactive conformation of RegX3s, we used MD simulation for 150 nanoseconds (ns) in explicit solvent condition and analyzed the convergence of conformational changes of RegX3 among MD trajectories with Principal Component Analysis (PCA), which analyzes total variance or mean-square displacement of atomic positional fluctuations in eight dimensional components (PCs). More than 60% of the variance was captured by the first two principal components (PCs), representing five major clusters of relatively stable structures (S1 Fig).

The simulated RegX3s adopts a reasonably compact conformation, which is clearly different from its original active state (rmsd of 12.5 Å for all C α atoms) (Fig 1A and S2 Fig). Globally, the ED swings 174° toward the RD with α 4 rotation of 51.6°, resulting in a compact conformation resembling MtrA and PrrA, when compared with the active RegX3 (S2A Fig). Partial helical unwinding and rotation of α 4 helix change its original perpendicular positioning to a position parallel to the RD of RegX3s as in PhoB, TorR, MtrA and YycF. The hydrophobic patches Val^{88, 89} and Leu⁹³ are protected by β 4 and β 5. In addition, the helical unwinding of α 4 leads two amino acids extension of loop β 4 α 4. Meanwhile, α 5 rotates 41° in the same direction as α 4, completing the α 4 β 5 α 5 face in an almost parallel conformation to both domains (Fig 1A). During the simulation, α 4 β 5 α 5 and the N-terminal region of α 1 appear to have significant conformational changes (Fig 1B and S3 Fig). In contrast, the ED keeps a rigid conformation as active RegX3 during simulation (rmsd of 1.2 Å for 96 C α atoms) (S2C and S2D Fig). The core α / β fold of the RD is even more rigid (rmsd of 0.76 Å for 74 C α atoms when aligned to active RegX3), which is also well conserved in inactive DrrD (PDB ID, 1KGS), BaeR (PDB ID, 4B09), MtrA (PDB ID, 2GWR) and PrrA (PDB ID, 1YS6) (rmsd of 0.9–1.5 Å).

Compact conformation of RegX3s is appropriate with tighter interdomain interactions than the active RegX3, which are mediated mainly by α 5 as well as loop β 5 α 5 of 11 residues in RD with α 7 and loop α 7 α 8 (transactivation loop) in ED (Fig 2). Asp¹²² interacts with Arg¹⁴² in RegX3s and Asp¹²¹ with Arg¹⁶⁷ in RegX3. Glu¹⁰⁷ keeps the same interaction with Lys¹⁵⁷ in both states. Arg¹¹³ interacts with Asp¹⁶⁰ in RegX3s but with Gly¹⁸⁴ in RegX3. The interdomain interface of inactive RegX3s is 868 Å², comparable with other inactive RRs, for examples, MtrA (738 Å²), PrrA (820 Å²), DrrB (751 Å²) and DrrD (245 Å²).

More importantly, the signature residue Tyr⁹⁸ of the α 4 β 5 α 5 face adopts an outward conformation as in inactive states of other RRs, while it flips without any rotameric changes to its coupling residue Thr⁷⁹ in original active RegX3. The side chain of the second signature switch residue Thr⁷⁹ adopts a new conformation that faces against the active pocket (Fig 1C). Together, we concluded that RegX3s has adopted a putative inactive conformation of RegX3 generated from MD simulation.

Conformational dynamics of loops

Several loops surrounding the active site were proposed to be vital for RR phosphorylation and global conformational changes [21]. In order to examine their dynamics in RegX3, the trajectories for β 1 α 1, β 3 α 3 and β 4 α 4 loops from both active and inactive states were assembled and analyzed in LigPlot⁺ and Bio3d.

Loops β 1 α 1 (amino acids 8–10) and β 4 α 4 (amino acids 79–82) stabilize the active RegX3 conformation through interactions with trivalent ions [13]. Loop β 1 α 1, composed of two glutamic acids and one aspartic acid, exhibits the least conformational fluctuation (rmsd of 0.5 Å for 3 C α atoms) during active to inactive transition (Fig 3A). In contrast, loop β 4 α 4, as a connection between α 4 β 5 α 5 face and the RD core region, shows a slightly larger conformational change (rmsd 0.8 Å for 4 C α atoms) (Fig 3C). Both loops form an interaction network with La³⁺ ion and water through Arg⁸¹, Glu⁸⁴, Glu¹⁰ and Asp⁹ together with Asp⁵² in active RegX3 (Fig 3D). However, significant conformational shift of loop β 4 α 4 in inactive RegX3s renders Arg⁸¹ to make two hydrogen bonds directly with Asp⁵² and projects Asp⁹ and Glu¹⁰ out of the phosphorylation site (Fig 3E). During transition the observed dynamics of these loops are in good agreement with previously published data (20, 36).

Taken together, these data from the MD simulation suggest that the loop β 4 α 4 extended from rotation and partial helical unwinding of α 4 causes Arg⁸¹ to establish a completely different interaction network in inactive RegX3s. It is interesting to note that loop β 3 α 3 (amino

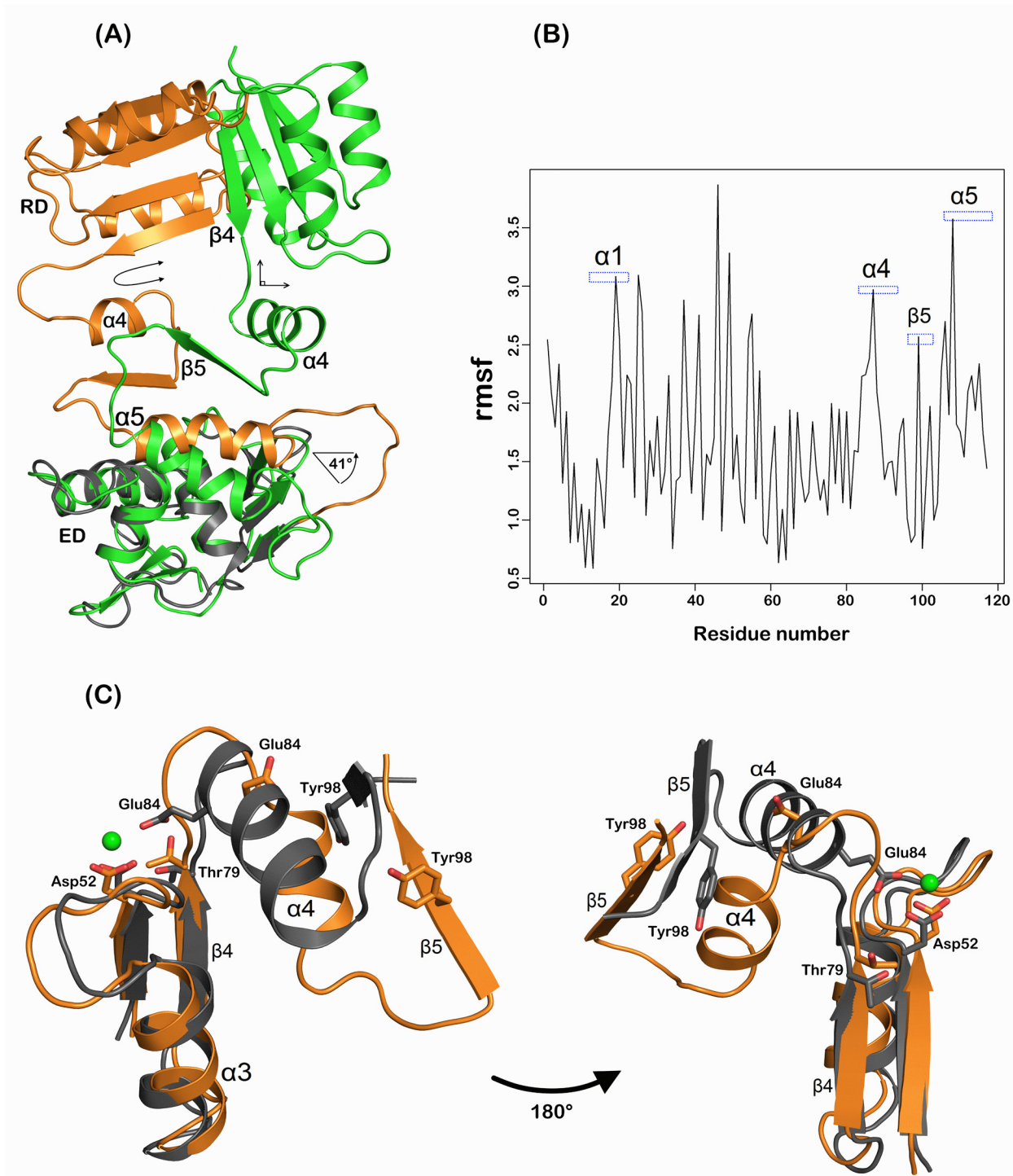


Fig 1. Conformational switch of RegX3 active Pocket in MD simulation. (A) Structural alignment of simulated RegX3s (colored in orange) and original active RegX3 (colored in green). The alignment was based on core folding of ED. $\alpha 4\beta 5\alpha 5$ face elements are labeled. Rotation degree of $\alpha 5$ is indicated with arrow in the lower half of the structure. Perpendicular and parallel switch for $\beta 4\alpha 4$ are marked in the upper half of the structure. (B) High mobility of RegX3 residues based root-mean-square fluctuation (rmsf). (C) Active pocket stabilized by key residues together with a lanthanum ion in the active conformation of RegX3 in comparison with simulated RegX3s. The alignment and color scheme are the same as panel A. Coupled residues Thr⁷⁹ and Tyr⁹⁸ together with other important residues around active site are labeled with sticks. The green sphere represents Lanthanum ion.

doi:10.1371/journal.pone.0133389.g001

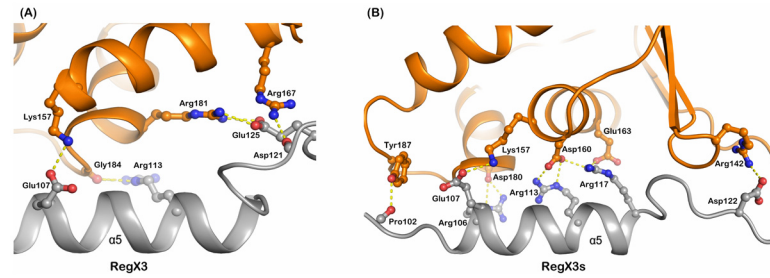


Fig 2. Interdomain interface between receiver and effector domains. Interdomain interactions between RD and ED domains of original active state (A) and simulated inactive state RegX3 (B) are shown in cartoon. The top half of each panel is from the ED in orange; the lower half is $\alpha 5$ and its adjacent loop in grey from the RD. Sticks represent all interaction residues with hydrogen bonds in yellow dotted lines.

doi:10.1371/journal.pone.0133389.g002

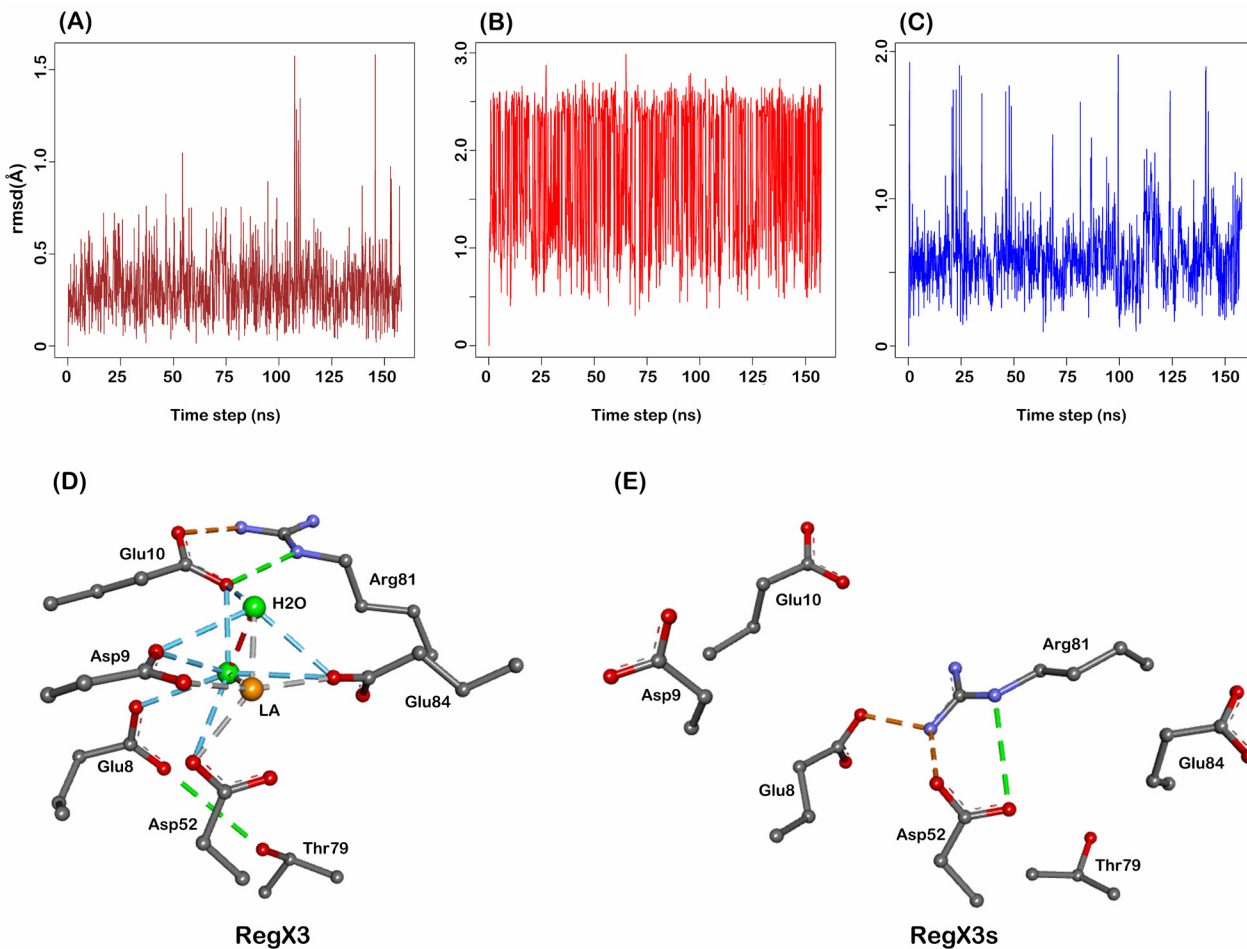


Fig 3. Dynamics of $\beta 1\alpha 1$, $\beta 3\alpha 3$ and $\beta 4\alpha 4$ loops. (A-C) rmsd deviation plots of $\beta 1\alpha 1$, $\beta 3\alpha 3$ and $\beta 4\alpha 4$ loops of RegX3 during 150 ns simulation. X-axis is time step and Y-axis indicates rmsd deviations. Interaction networks of these loops are explicated in active state (D) and inactive state (E). Residues are shown in ball and sticks. Brown and green spheres indicate La^{3+} ion and water molecule, respectively. All interactions are highlighted in dashed lines.

doi:10.1371/journal.pone.0133389.g003

acids 53–59) exhibits the most conformational fluctuations (rmsd of 2.0 Å for 7 C α atoms) among these three loops during the active-inactive transition (Fig 3B), but it does not appear to change the interaction network in phosphorylation site (Data not shown).

Conformation transition network

Low frequency normal mode analysis (NMA) of elastic network model (ENM) is a preferable approach to capture long-range conformational change, which is otherwise very expensive for MD [24–26]. The low frequency NMA modes depict the functional relevance. The estimated collective parameters of motions were calculated for the active to inactive transition of RegX3. The collective overlap score for the first 10 modes was 0.95, which was dominated by mode 2 (the core of 0.84), indicating that the transition of RegX3 structures is functionally relevant (Fig 4A).

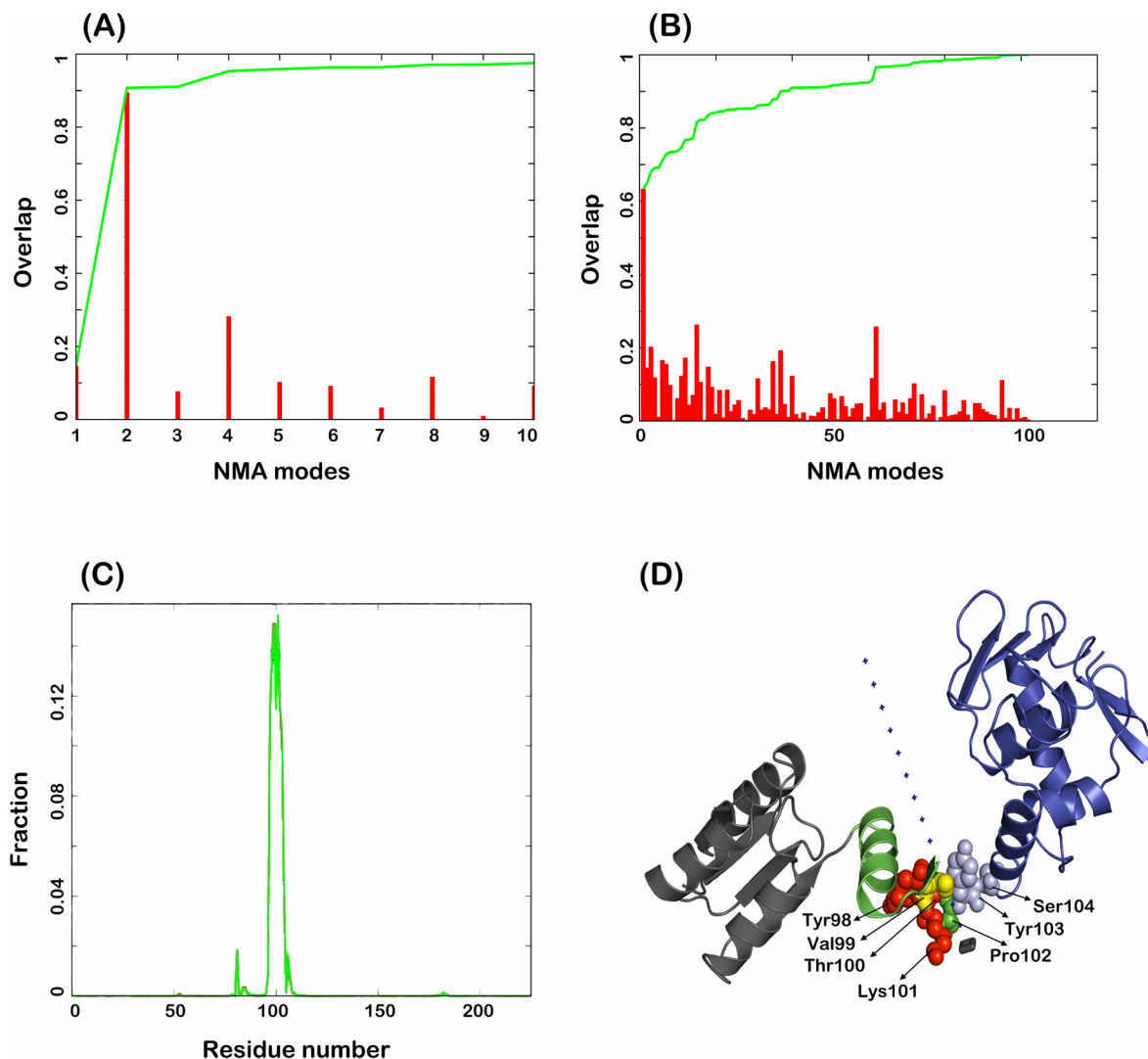


Fig 4. Normal model analysis for conformational dependent regions of RegX3. (A) Overlap score of all non-zero low frequency modes between active and inactive state structures. (B) Overlap score of non-zero ENM modes based on the contribution of pocket residues of $\alpha 4\beta 5\alpha 5$ face to the overall changes of full-length RegX3. (C) Contribution fraction (Y-axis) of residues to low frequency NMA modes in pocket residue analysis. (D) Key structural region with the nature of individual residues contributes to conformational changes during active to inactive transition of RegX3. ED is colored in grey and RD in blue. Helix $\alpha 4$ is colored in green and hot spot residues are in sphere models. The direction of an arrow represents the hinge motion of blue (ED) towards black (RD).

doi:10.1371/journal.pone.0133389.g004

The NMA non-zero mode 2 revealed a closure rotation of RD towards ED using a hinge region $\alpha 4\beta 5$, suggesting that $\alpha 4\beta 5$ effectively controls the fluctuation of RegX3. To investigate dependency of the total overlap on $\alpha 4\beta 5\alpha 5$ face during the active to inactive transition, we performed NMA again using $\alpha 4\beta 5\alpha 5$ face as a pocket region. The initial modes were dominant and scored approximately 0.64, suggesting dependency of the $\alpha 4\beta 5\alpha 5$ face in RegX3 conformational transitions (Fig 4B). Consistently, the coherent nature of the pocket residue analysis further indicated an importance of the $\alpha 4\beta 5$ region but not $\alpha 5$ in RegX3 function (Fig 4C). It is interesting that this analysis also showed a relatively small signal for Asp⁸². To further refine $\alpha 4\beta 5$ as a critical region in transition, we performed a hot-spot analysis. Residues Tyr⁹⁸ to Ser¹⁰⁴ in RegX3 exhibited high $\sigma\omega$ value in the overall elastic distortion, and thus considered as the “hot-spot” residues (Fig 4D).

These hot-spot residues may likely be important to modulate global dynamics between active and inactive states of RRs in long-range conformational communications. Tyr⁹⁸ has been shown to play a key role in allosteric transition of OmpR/PhoB family whereas Lys¹⁰¹ interacts with the side chain of Thr⁷⁹ only in active RR [3, 13]. Taken together, our NMA analysis indicates that residues Tyr⁹⁸ to Ser¹⁰⁴ of $\alpha 4\beta 5$ region are the most important in RegX3 conformational switch.

Coevolution analysis

We next performed a coevolution analysis to search for critical residues connecting the dimeric interface and global conformational changes. We collected 29,283 members of OmpR/PhoB family and analyzed them using a program GREMLIN, which constructs a global statistical model, assigns probability to each residue and calculates all evolving positions (Fig 5). The top 23 pairs of coevolved residues involved in dimeric interface were selected within the cutoff distance of 5 Å (Table 1).

We then compared these coevolved residues in RegX3, PhoB (1ZES), TorR (1ZGZ) and YycF (1NXP) in OmpR/PhoB family. Residues of 19 pairs were involved only in stabilization of RegX3 dimer and not of PhoB, TorR and YycF, which were therefore excluded from our analysis (Table 1, italicized). The remaining four pairs are conserved in dimer interfaces of active PhoB, TorR and YycF (Fig 6). Lys⁸⁷-Glu¹⁰⁷ pair does not contribute to RegX3 dimerization although it surely is one of key residues in PhoB, TorR and YycF. In contrast, Asp⁹⁷-Arg¹¹¹ pair is an important player in RegX3 since it stabilized conformation of $\beta 5$ and $\alpha 5$ by a salt bridge [14]. Therefore, Glu²⁴-Arg¹¹³, Asp⁹⁷-Arg¹¹¹ and Ile⁷⁶-Asp⁹⁶ were critical residues to connect the dimeric interface with global conformational changes during active to inactive transition of RegX3.

In silico mutagenesis

To further study these coevolved residues on RegX3 conformational changes, we subjected the active RegX3 with a series of alanine mutations for residues Glu²⁴, Ile⁷⁶, Asp⁹⁶, Asp⁹⁷, Arg¹¹¹ and Arg¹¹³ to 5 ns MD simulation. The original active RegX3 was also set up to generate RegX3-5ns as a control. Trajectories from these MD simulations were assembled by Nosé-Hoover constant pressure and temperature (NPT) system, and analyzed by PCA for variances of the first 2 PCs, leading to estimation of mutational effects for these single or double mutations (S4 Fig). RegX3-5ns maintains the same trajectory of $\alpha 4$ and $\alpha 5$, but $\beta 5$ and $\alpha 5$ parallel shift about 8 Å (S5A Fig). In contrast, mutant mRegX3(96) shows 31° rotation and 13 Å parallel shift of $\beta 5$ while mRegX3(76,96) has nearly 120° rotation of $\beta 5$ and $\alpha 5$ in addition to 46° rotation of $\alpha 4$ (S5B and S5C Fig). All secondary structures of $\alpha 4\beta 5\alpha 5$ have as large as 30–75° rotations in mRegX3(97), mRegX3(111) and mRegX3(97,111), which are not observed in RegX3-

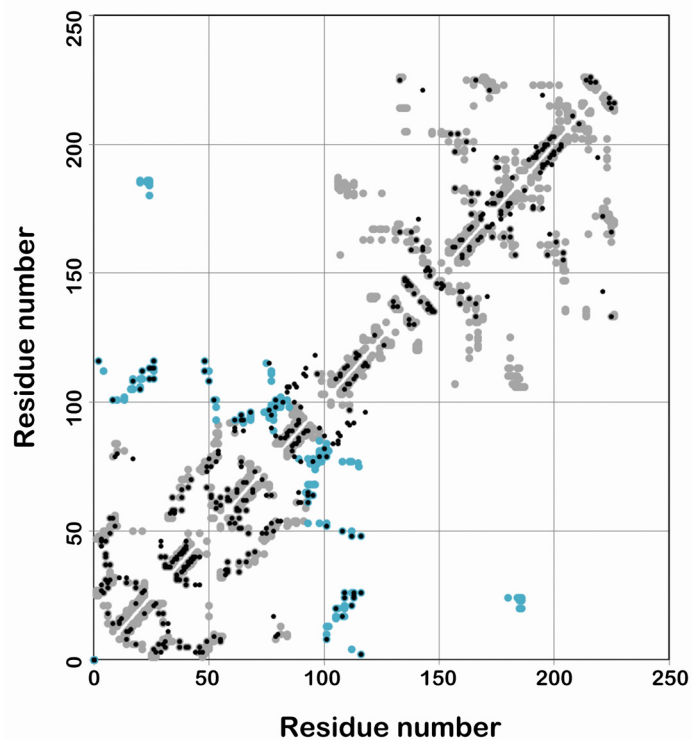


Fig 5. Coevolution analysis of RegX3. Contact map of coevolved residues in OmpR/PhoB family. Axes are residue numbers. Grey spots represent contacts within the same monomer, while black spots are predicted inter-monomeric contacts. The blue spots highlight those coevolved pairs in dimeric interface listed in [Table 1](#).

doi:10.1371/journal.pone.0133389.g005

5ns ([S5D](#), [S5E](#) and [S5F](#) Fig). More dramatically, $\alpha 4\beta 5\alpha 5$ all switch into perpendicular positions in mRegX3(113) and shift 68° in addition to a large rotation in mRegX3(24,113) ([S5G](#) and [S5H](#) Fig). It is noteworthy that Ile⁷⁶ is important to mediate domain-swapped dimer only in RegX3 but not for other OmpR/PhoB family [13]. Together, all these mutations seem to release constraints on conformation of $\alpha 4\beta 5\alpha 5$ region compared with wild-type RegX3 in our MD experiments, suggesting that these key residues identified from the coevolution analysis are indeed important for RegX3 structural dynamics.

We then analyzed these structures of RegX3 mutants for global conformational changes with OmpR/PhoB family members using *Bio3d* [27] and differences in these structures were presented in PCA planes ([Fig 7A](#)). DrrB and DrrD form one inactive group with an extended conformation. The simulated RegX3s is clustered next to PrrA and MtrA as another inactive group with a compact conformation, whereas RegX3 clusters with RegX3-5ns, retaining an active group. The mutants mRegX3(96), mRegX3(97), mRegX3(111), mRegX3(97,111) and mRegX3(76,96) are clustered near the active group. Interestingly, mRegX3(113) and mRegX3(24,113) appear to attain a transitional conformation between the active and inactive groups.

Together, our *in silico* mutagenesis experiments indicates different effects of these coevolved residues on conformational changes of RegX3. The conservation of these coevolved residues depicts their importance for OmpR/PhoB family. Interestingly, the residues responsible for these structural distributions are in N-terminal RD rather than C-terminal ED ([Fig 7B](#)), further signifying the dominant role of RD in regulating the global conformation of a RR.

Table 1. Coevolved residues of dimer interface of OmpR/PhoB family calculated by GREMLIN: Listed are the interacting residues with their respective numberings and topology. Italicized pairs indicate coevolved inter-monomeric contacts of RegX3 but intra-monomeric contacts in other OmpR/PhoB family members. Bold representation highlights those dimeric interactions conserved in all OmpR/PhoB family members. Contact pair with asterisk symbol satisfies all available active RR structures in this family but not RegX3.

Observed_score	Partner 1	Partner 2	Topology
2.026	<i>Leu20</i>	<i>Ala105</i>	$\alpha1$ - $\alpha5$
2.162	Lys87*	Glu107*	$\alpha4$ - $\alpha5$
1.73	<i>Ile48</i>	<i>Leu112</i>	$\beta3$ - $\alpha5$
1.715	<i>Leu21</i>	<i>Leu112</i>	$\alpha1$ - $\alpha5$
1.526	Asp97	Arg111	$\beta5$-$\alpha5$
1.441	<i>Arg68</i>	<i>Asp96</i>	$\alpha3$ - $\beta5$
1.354	<i>Glu24</i>	<i>Ile109</i>	$\alpha1$ - $\alpha5$
1.315	<i>Thr61</i>	<i>Leu93</i>	$\alpha3$ - $\alpha4$
1.206	<i>Phe26</i>	<i>Arg113</i>	$L2$ - $\alpha5$
1.155	<i>Ile48</i>	<i>Leu116</i>	$\beta3$ - $\alpha5$
0.983	<i>Leu17</i>	<i>Leu108</i>	$\alpha1$ - $\alpha5$
0.955	<i>Phe26</i>	<i>Leu109</i>	$L2$ - $\alpha5$
0.896	Glu24	Arg113	$\alpha1$- $\alpha5$
0.869	Ile76	Asp96	$\beta4$- $\beta5$
0.866	<i>Asp82</i>	<i>Thr100</i>	$L7$ - $\beta5$
0.834	<i>Lys65</i>	<i>Leu93</i>	$\alpha3$ - $\alpha4$
0.831	<i>Glu8</i>	<i>Lys101</i>	$L1$ - $\beta5$
0.826	<i>Thr2</i>	<i>Leu116</i>	$\beta1$ - $\alpha5$
0.801	<i>Leu50</i>	<i>Leu108</i>	$\beta3$ - $\alpha5$
0.79	<i>Thr79</i>	<i>Lys101</i>	$\beta4$ - $\beta5$
0.777	<i>Cys64</i>	<i>Ala95</i>	$\alpha3$ - $\beta5$
0.754	<i>Asp52</i>	<i>Lys101</i>	$\beta3$ - $\beta5$
0.722	<i>Phe26</i>	<i>Leu116</i>	$L2$ - $\alpha5$

doi:10.1371/journal.pone.0133389.t001

Discussions

In OmpR/PhoB family, phosphorylation actuates dimerization through two possible pathways: rearrangement of RD and ED domains that overcomes dimerization inhibition and subtle conformation changes of some critical residues at the dimer interface [28, 29]. However, connections between these two pathways in conformational dynamics of a RR have not been thoroughly investigated. In this study we generated an inactive state of RegX3, a RR in OmpR/PhoB family through 150 ns MD and compared it with its original active state by a variety of computational analyses. Further analysis by coevolution identified several critical interaction residues, which were fully supported by *in silico* mutagenesis. All these portray a coherent picture of molecular dynamics of OmpR/PhoB family during active to inactive transition.

Conformational dynamics of RegX3

Inactive state of RegX3 generated from 150 ns MD has a compact global conformation and typical rotameric conformation of Tyr⁹⁸ and Thr⁷⁹ as other inactive RRs (Figs 1 and 2). A hinge motion of $\alpha4\beta5$ region bears a sufficient flexibility for RegX3 to mediate the active to inactive transition process (Fig 4). Indeed, phosphorylation of NtrC, FixJ, DctD, Spo0F and PhoB has been shown to induce conformational changes mainly in loop $\beta4\alpha4$ and helix $\alpha4$ [30–34]. $\alpha4$ is also structurally unstable in other RRs such as CheY, DrrD and BaeR [10, 11, 35]. In RegX3, helix $\alpha4$ adopts a perpendicular position that is closer to DrrD and BaeR, however in inactive

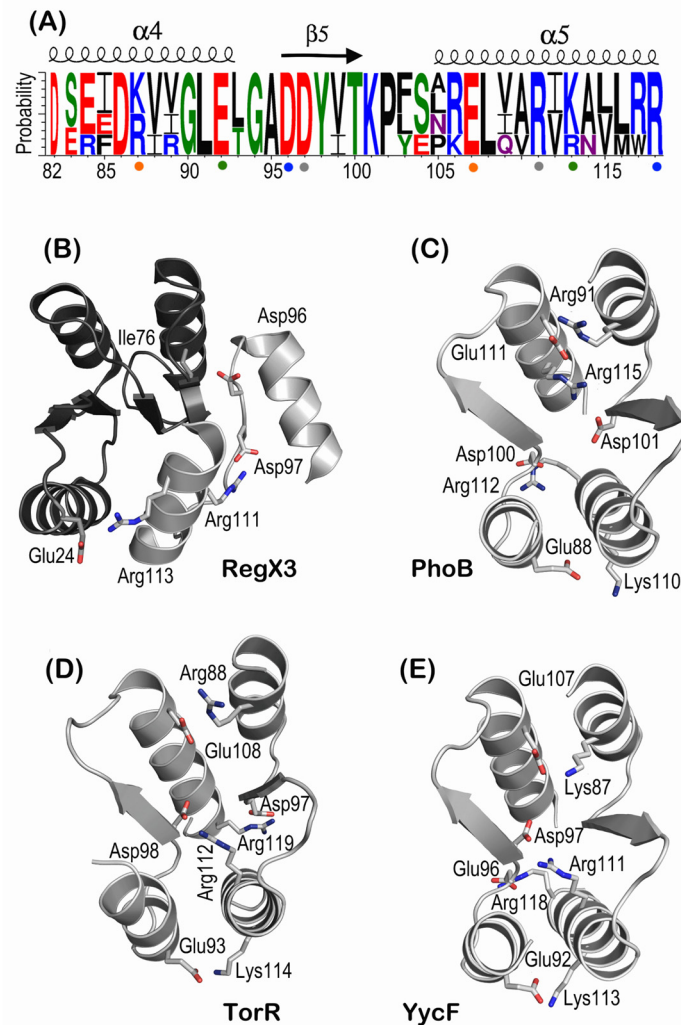


Fig 6. Coevolved residues in dimeric interface of OmpR/PhoB family. (A) Sequence conservation of the $\alpha 4\beta 5\alpha 5$ dimeric interface of RegX3, PhoB, TorR and YycF in OmpR/PhoB family. Residues are numbered according to RegX3 and colored based on chemistry: acidic in red, basic in blue, hydrophobic in black, polar in green and neutral in purple. Coevolved pairs are under-dotted with the same colors. (B-E) Active state structures of RegX3 (2OQR), TorR (1ZGZ), PhoB (1ZES) and YycF (1NXP) in OmpR/PhoB family with coevolved residues in dimeric interface highlighted in sticks. It is noteworthy that RegX3 forms a complete dimeric structure with swapped domains that are colored in light and dark greys.

doi:10.1371/journal.pone.0133389.g006

state it rotates 51.6° occupying a parallel position to the core RD as in PrrA and MtrA [12, 15]. The rotation of $\alpha 4$ is accompanied by $\beta 4\alpha 4$ loop that subsequently exposes Thr⁷⁹ and partially Tyr⁹⁸ as in inactive DrrD (Fig 1C). Such inactive rotameric state of Tyr⁹⁸ has been suggested as the third state for inactive RRs [17].

Loop $\beta 4\alpha 4$ is shown with more dramatic conformational changes than loop $\beta 1\alpha 1$ and $\beta 3\alpha 3$ during active to inactive transition, which breaks down the interaction network built by Thr⁷⁹, Glu⁸, Glu¹⁰, Asp⁵² and Glu⁸⁴ together with Arg⁸¹. Consequently, the conserved Arg⁸¹ replaces its interaction partner with Glu⁸ and Asp⁵² to achieve the inactive state (Fig 3). On the other hand the re-positioning of Arg⁸¹, Asp⁹ and Glu¹⁰ in inactive state allows 5.7° rotation of N-terminal helix $\alpha 1$ (S3 Fig). A slow motion of helix $\alpha 1$ has been shown critical for interactions

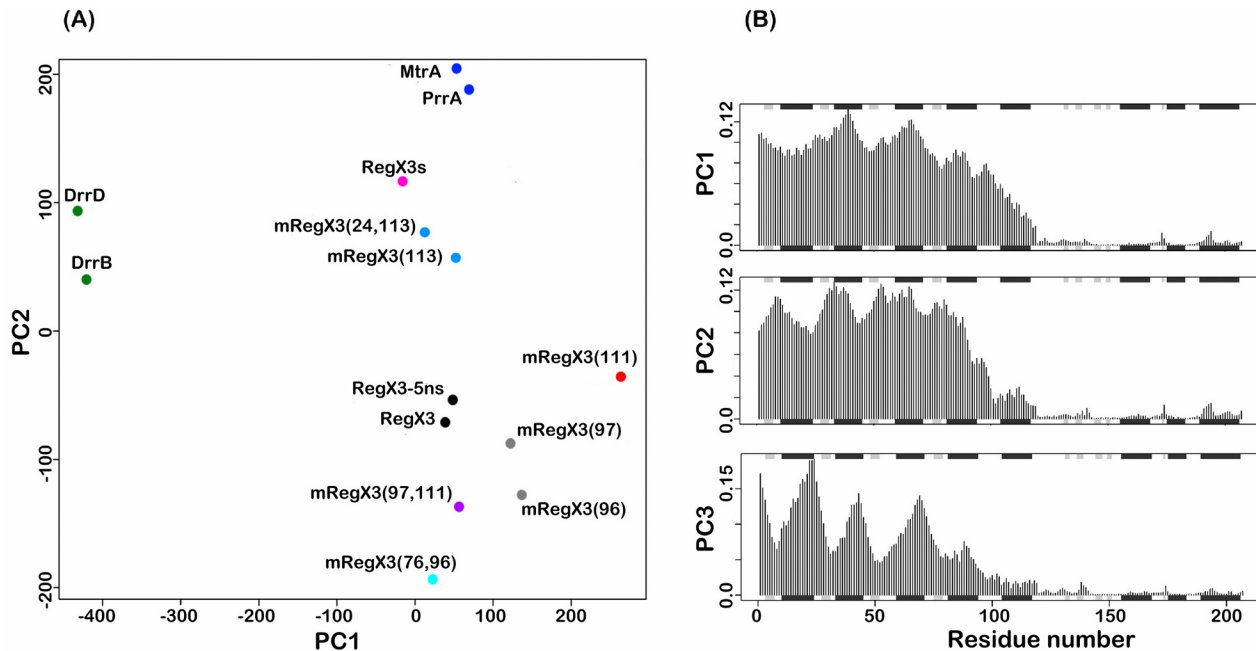


Fig 7. In silico mutagenesis analysis of RegX3. (A) Simulated structures of active RegX3 with introduced mutations are analyzed by PCA. RegX3s and RegX3-5ns used as a control are those simulated structures after 150 ns and 5 ns, respectively. mRegX3 indicates RegX3 mutant simulated for 5 ns with numbers in parenthesis for alanine mutation of specific sites. DrrB and DrrD are representative inactive and open RR structures with exposed DNA recognition helices. MtrA and PrrA are representative inactive and compact structures with buried DNA recognition helices. Structures are grouped by color dots. (B) The frequency distribution of individual residues contributing to all RegX3 structures on PC spaces. Y-axis indicates the observed frequency and X-axis represents the residue numbers of RegX3. Grey and black color regions on the X-axis indicate β sheets and α helices whereas the white spaces in between indicate loop regions.

doi:10.1371/journal.pone.0133389.g007

with KinA, Spo0B and RapB [36]. In addition, these loops stabilize the phosphorylatable Asp⁵² in active state of RegX3, which is important in dephosphorylation for specific recognition by sensor histidine kinases [37, 38]. The re-orientations of Thr⁷⁹, Arg⁸¹ and Glu⁸⁴ render $\alpha 4$ in a parallel position to the core RD, which is further supported by the 41° axial rotation of $\alpha 5$ that secures a compact conformation of RegX3s through new contacts of Arg¹¹³ and Asp¹⁶⁰, Arg¹⁰⁶ and Asp¹⁸⁰ and Arg¹¹⁷ and Glu¹⁶³ on inter-domain interface (Fig 2B). At sub-family level of RRs (OmpR/PhoB), Arg¹¹³ is an evolutionary conserved residue of dimeric interface (Fig 6A) and interacts with Glu⁹² in active state dimer.

The dynamic relevant hot-spots residues may probe specific responses to induce local changes that mediate signal transmission. A cluster of seven hot spots (Tyr⁹⁸ to Lys¹⁰¹) with high $\delta\omega$ values, containing C terminal half of $\beta 5$ and its adjacent loop, are defined as most critical residues in active-inactive transition. Consistently, Tyr⁹⁸ and Lys¹⁰¹ have been shown important to maintain a stable environment for phosphorylation site in OmpR/PhoB family [13, 39–41]. The $\alpha 5$ is less important but may possibly involve in interdomain interaction of RegX3 to form a compact conformation (Fig 2).

Critical residues on dimer interface

Last decade has seen considerable effect to study residue-residue contacts by covariation from aligned sequences using direct-coupling information and inverse-covariance, e.g. Direct Coupling Analysis (DCA) and Protein Sparse Inverse COVariance (PSICOV) [42, 43]. GREMLIN program recently developed by Baker and his colleague obtains model parameters from conditional correlations with fewer sets of protein sequences using a frame work of pseudo-

likelihood integrated with structural information [44]. The authenticity of GREMLIN was tested using a crystal structure of VicK [45] and its homologues (data not shown), which demonstrated its efficiency to capture co-evolutionary signals in both active and inactive states of sensor histidine kinases as DCA [42, 46].

The $\alpha 4\beta 5\alpha 5$ region is important for transition from inactive to active state [47, 48]. The specificity of homo- and hetero-dimer interface in OmpR/PhoB has been demonstrated by Förster resonance energy transfer (FRET) analysis [49]. Our coevolution analysis suggested that the specificity of dimeric interface in OmpR/PhoB family is evolutionarily optimized (Fig 6). We identified 23 coevolved pairs involved in the dimer interface with top scores (Table 1). Three pairs of Glu²⁴-Arg¹¹³, Asp⁹⁷-Arg¹¹¹ and Ile⁷⁶-Asp⁹⁶ were selected as critical residues for RegX3 after excluding all intra-monomeric contacts. Mutations of these residues altered the dynamics of global conformation of RegX3 (Fig 7 and S5 Fig). Consistently, Arg^{113A/E} mutation (Arg¹¹¹ in RegX3) abolished the dimer formation of active state PhoP *in vivo*. Single mutation Arg^{115D} dramatically decreased PhoB DNA binding and transcriptional activities, which were partially rescued by compensatory mutation Asp^{101R} (Asp⁹⁶ and Arg¹¹¹ in RegX3) [50]. Altogether, this data further substantiate that $\alpha 4\beta 5\alpha 5$ face is critical for RR conformational change and dimerization during active to inactive transition.

Summary

RRs are sensitive to phosphorylation-induced conformational changes. Phosphorylated RRs are stabilized by divalent ions like Ca²⁺ or Mg²⁺, which utilize binding sites from $\beta 1\alpha 1$ and $\beta 4\alpha 4$ loops. In active state these proximal loops are in stretched conformation and face the C-terminus of $\beta 3$. The absence of divalent and phosphate ions from the active pocket remodeled $\beta 1\alpha 1$ loop from a stretched to a relaxed conformation resulting the outward orientation of Glu¹⁰ and Asp⁹ that is supported by Arg⁸¹ from $\beta 4\alpha 4$ loop. Arg⁸¹ breaks its contacts with the loop $\beta 1\alpha 1$ to establish a new interaction network with the phosphorylatable aspartate, which possibly promotes an outward movement of N-terminal helix $\alpha 1$. The hot-spot cluster of $\alpha 4\beta 5$ is most critical in maintaining the active/inactive conformation of a RR. All in all, these studies suggest a general working model for OmpR/PhoB family in which the $\alpha 4\beta 5$ region with several coevolved residues together with Arg⁸¹ are pivotal for global and local structural dynamics that govern the active to inactive conversion induced by RR phosphorylation state.

Methods

Coevolution analysis

A total of 29,283 sequences (The alignment file is available upon request) of all full length response regulators were gathered and an alignment was constructed using HHblits server [51]. The aligned sequences [X₁, X₂, X₃,...,X_p] with positions 1:p, were filtered by removing those sequences with >90% identity and more than 75% gaps. A program GREMLIN was used to extract all possible coevolution signals. The reduction of w_{ij} matrices to single values reflects the total strength of the coupling between positions i and j. We first computed s_{ij}, their vector 2-norm (the square root of the averages of the squares of the individual matrix elements) and corrected differences in s_{ij} due to sequence variability using the row and column averages of these values:

$$S_{ij}^{corr} = S_{ij} - \frac{\langle S_{kj} \rangle_k \langle S_{ik} \rangle_k}{\langle S_{kl} \rangle_{kl}}$$

The brackets represent averages taken over the indices outside the brackets in a manner similar to Average Product Correction (APC) [52]. The normalized coupling strength or “scaled score”, ncs_{ij} , was computed by dividing the S_{ij}^{corr} value by the total average of the top $3L/2$ S_{ij}^{corr} values (since there are roughly $3L/2$ contacts for a protein of length L [44]).

Gremlin model construction from paired alignments

GREMLIN constructs a global statistical model, and assigns a probability to every amino-acid in an alignment:

$$p(X_1, X_2, \dots, X_p) = \frac{1}{Z} \exp(\sum_1^p [v_i(X_i) + \sum_{j=1}^p w_{ij}(X_i, X_j)])$$

where v_i are vectors encoding position-specific amino acid propensities and w_{ij} are matrices encoding the coupling of amino acids between positions i and j . All these parameters are determined by maximizing the regularized pseudo-likelihood of the sequence alignment as described in [44, 53].

$$v, w = \operatorname{argmax}_{\Sigma_1^N} \sum_1^p \log P(X_i | X_1 \dots X_{i-1} X_{i+1} \dots X_p) + R(v, w)$$

Where each summation is a conditional distribution capturing the probability of an amino acid at particular position in context of protein sequences. Regularization term $R(v, w)$ is used to prevent over-fitting.

Molecular dynamics

NAMD 2.10 (Beckman Institute, University of Illinois) was used to generate ensemble trajectories of RegX3 [54]. All individual MD simulations were performed in explicit solvent system with constant parameters. Protein structure files (psf) were generated using CHARMM36ff [55]. The whole system was neutralized by NaCl and solvated in an 8 Å cubic box. The default configuration settings were used with $1/\text{Å}^3$ PME grid density. Short-range, non-bonded interactions were calculated using a distance cut-off of 12 Å. The system was minimized for 1000 steps and simulated in the NPT ensemble ($T = 310$ K, $P = 1$ atm) with periodic boundary conditions having full particle-mesh Ewald electrostatics. Ligplot+ was used to analyze intra-protein contacts in active and inactive states of RegX3 [56]. Mutations were introduced into RegX3 structure using Modeller [57]. All structural illustrations were prepared in Pymol (DeLano Scientific LLC).

Principal Component Analysis

To compare different MD conformation, we performed principal component analysis (PCA) using a package Bio3d [27]. PCA is a multivariate technique, which minimizes the maximal variance of the data to two or three dimensions through examining inter-conformer relationships, based on the covariance matrix, C , with two elements i and j originates from the Cartesian coordinates of the all superposed structures.

$$C_{ij} = \langle (X_i - \langle X_i \rangle)(X_j - \langle X_j \rangle) \rangle$$

Where X is the mass weighted Cartesian coordinate of an N -particle system and C_{ij} represents an average of all sampled structures. The C matrix can be diagonalized with orthonormal transformation matrix R :

$$R^T C R = \operatorname{diag}(\lambda_1, \lambda_2, \dots, \lambda_{3N})$$

T is transpose of R and $\lambda_1 \geq \lambda_2 \geq \dots \geq \lambda_{3N}$ indicates eigenvalue. To obtain the principal components $q_i(t)$, $i = 1, \dots, 3N$, the trajectories can be projected on the eigenvectors in the columns of R.

$$q = R^T(x(t) - \langle x \rangle)$$

In the direction of principal mode, the eigenvalue λ_1 is the mean square fluctuation. In PCA the first few PCs normally show global motions and contain the largest root mean square fluctuation.

Elastic Network Model (ENM)

Elastic potentials of C α coordinates of both active and inactive RegX3 as elastic bodies were constructed with a force constant of C indicating pair wise interaction of C α atoms within R_c cut-off distance. The resultant potential energy of the elastic network is expressed as:

$$E(x^{\rightarrow} - x_o^{\rightarrow}) = \frac{1}{2} \sum_{d_{ij}^o < R_c} C(d_{ij} - d_{ij}^o)^2$$

Where x is a 3N-dimensional vector representing Cartesian coordinates of RegX3 C α atoms and x_o is a corresponding vector indicating C α positions in RegX3 structure. d_{ij}^o and d_{ij} represent the corresponding distance between two structures and two C α atoms at positions i and j, respectively.

The above equation of potential energy calculation for elastic network is expanded to its second order by computing its Hessian matrix H, which best describes large amplitude motions in a protein for low frequency normal modes [58]:

$$E(\delta x^{\rightarrow}) \approx \frac{1}{2} \delta x^{\rightarrow T} \cdot H \cdot \delta x^{\rightarrow}$$

MENM potential functions of RegX3 were calculated as Best et al [59]:

$$E(x^{\rightarrow}) = -\beta^{-1} \ln[e^{-\beta(E1(x^{\rightarrow} - x_1^{\rightarrow}) + \epsilon_1)} + e^{-\beta(E2(x^{\rightarrow} - x_2^{\rightarrow}) + \epsilon_2)}]$$

Where ϵ_1 and ϵ_2 indicate energy off-sets and β is T_m/k_B , inverse of mixing temperature. E_1 and E_2 were calculated for two MENM low frequency modes of RegX3 active and inactive states with Hessian matrix.

To detect hot spot residues, response of harmonic spring to perturbation in frequency of mode M was calculated as:

$$\delta\omega(M, n) = VMT \cdot \delta H \cdot VM \cdot \delta H$$

Where VM represents the eigenvector of mode M at residue position n and δH is the observed change of Hessian matrix to the energy of elastic network. $\delta\omega(M, n)$ indicates sensitivity of mode M to hot spot residues which illustrates evolutionary conservation and functional relevance [25].

Supporting Information

S1 Fig. Projection of clustered conformers on to the principal components obtained from 150 ns MD trajectories of RegX3. The contribution pattern and variance in the MD trajectories are presented in clusters with different colors in PC1, PC2. Cyan represents the first cluster followed by black, green, blue and red. Members from the respective cluster are shown with the same color. The clustering was made with 100 strides from MD trajectories that explain the behavior of conformational transition of RegX3.

(TIF)

S2 Fig. Angular rotation of the effector domain (ED). (A). Original active state RegX3 (green) and simulated RegX3s (RD; grey, ED; orange) are aligned using core RD. A closer rotation of ED (174°) and 51.6° downward shift of helix $\alpha 4$ is shown. (B). Time series for rmsd difference in MD trajectories. (C). Superimposition of ED from MD conformers. Different colors correspond to the clusters made in [S1 Fig.](#) (D). RMSF representation of the ED in MD simulation.

(TIF)

S3 Fig. Helix $\alpha 1$ outward shift. Structure alignment of rigid secondary structure elements of the RD of RegX3 (grey) and RegX3s (orange) is shown highlighting the 5.7° rotation and slight movement of N-terminal region of helix $\alpha 1$.

(TIF)

S4 Fig. Projection of clustered conformers on to the principal components obtained from 5 ns MD trajectories of mutant RegX3. (A-H) Distinct contributions of mutants MD trajectories highlighting conformational paths are shown in different colors on PC planes.

(TIF)

S5 Fig. Global scale effects on dimeric surface. (A-H) Impact of given mutation on dimeric interface are shown. Grey and orange colors designate 0 ns and the given mutant structure.

(TIF)

Acknowledgments

We are thankful to Mr. Sergey Ovchinnikov, University of Washington, USA for his intellectual discussion on GREMLIN program and coevolution data analysis. Mr. Hussain Ahmad, University of engineering and technology, Pakistan for sharing his mathematical understandings and Mr. Yandong Huang, Xiamen University, China for critical reading of the manuscript.

Author Contributions

Conceived and designed the experiments: AH. Performed the experiments: AA XC YC. Analyzed the data: AA. Contributed reagents/materials/analysis tools: AA YC XC AH JS. Wrote the paper: AA AH.

References

1. Letunic I, Copley RR, Pils B, Pinkert S, Schultz J, Bork P. SMART 5: domains in the context of genomes and networks. *Nucleic Acids Res.* 2006; 34(Database issue):D257–60. doi: [10.1093/nar/gkj079](https://doi.org/10.1093/nar/gkj079) PMID: [16381859](https://pubmed.ncbi.nlm.nih.gov/16381859/); PubMed Central PMCID: PMC1347442.
2. Gao R, Stock AM. Evolutionary tuning of protein expression levels of a positively autoregulated two-component system. *PLoS Genet.* 2013; 9(10):e1003927. doi: [10.1371/journal.pgen.1003927](https://doi.org/10.1371/journal.pgen.1003927) PMID: [24204322](https://pubmed.ncbi.nlm.nih.gov/24204322/); PubMed Central PMCID: PMC3812086.
3. Robinson VL, Buckler DR, Stock AM. A tale of two components: a novel kinase and a regulatory switch. *Nature structural biology.* 2000; 7(8):626–33. doi: [10.1038/77915](https://doi.org/10.1038/77915) PMID: [10932244](https://pubmed.ncbi.nlm.nih.gov/10932244/).
4. Smith JG, Latiolais JA, Guanga GP, Pennington JD, Silversmith RE, Bourret RB. A search for amino acid substitutions that universally activate response regulators. *Molecular microbiology.* 2004; 51(3): 887–901. PMID: [14731287](https://pubmed.ncbi.nlm.nih.gov/14731287/).
5. Porter SL, Wadhams GH, Martin AC, Byles ED, Lancaster DE, Armitage JP. The CheYs of *Rhodobacter sphaeroides*. *The Journal of biological chemistry.* 2006; 281(43):32694–704. doi: [10.1074/jbc.M606016200](https://doi.org/10.1074/jbc.M606016200) PMID: [16950782](https://pubmed.ncbi.nlm.nih.gov/16950782/).
6. Parish T, Smith DA, Roberts G, Betts J, Stoker NG. The *senX3-regX3* two-component regulatory system of *Mycobacterium tuberculosis* is required for virulence. *Microbiology.* 2003; 149(Pt 6):1423–35. PMID: [12777483](https://pubmed.ncbi.nlm.nih.gov/12777483/).

7. Glover RT, Kriakov J, Garforth SJ, Baughn AD, Jacobs WR Jr. The two-component regulatory system senX3-regX3 regulates phosphate-dependent gene expression in *Mycobacterium smegmatis*. *Journal of bacteriology*. 2007; 189(15):5495–503. doi: [10.1128/JB.00190-07](https://doi.org/10.1128/JB.00190-07) PMID: [17526710](https://pubmed.ncbi.nlm.nih.gov/17526710/); PubMed Central PMCID: PMC1951828.
8. Roberts G, Vadrevu IS, Madiraju MV, Parish T. Control of CydB and GltA1 expression by the SenX3 RegX3 two component regulatory system of *Mycobacterium tuberculosis*. *PLoS One*. 2011; 6(6): e21090. doi: [10.1371/journal.pone.0021090](https://doi.org/10.1371/journal.pone.0021090) PMID: [21698211](https://pubmed.ncbi.nlm.nih.gov/21698211/); PubMed Central PMCID: PMC3116866.
9. Blanco AG, Sola M, Gomis-Ruth FX, Coll M. Tandem DNA recognition by PhoB, a two-component signal transduction transcriptional activator. *Structure*. 2002; 10(5):701–13. PMID: [12015152](https://pubmed.ncbi.nlm.nih.gov/12015152/).
10. Buckler DR, Zhou Y, Stock AM. Evidence of intradomain and interdomain flexibility in an OmpR/PhoB homolog from *Thermotoga maritima*. *Structure*. 2002; 10(2):153–64. PMID: [11839301](https://pubmed.ncbi.nlm.nih.gov/11839301/).
11. Choudhury HG, Beis K. The dimeric form of the unphosphorylated response regulator BaeR. *Protein science: a publication of the Protein Society*. 2013; 22(9):1287–93. doi: [10.1002/pro.2311](https://doi.org/10.1002/pro.2311) PMID: [23868292](https://pubmed.ncbi.nlm.nih.gov/23868292/); PubMed Central PMCID: PMC3776340.
12. Friedland N, Mack TR, Yu M, Hung LW, Terwilliger TC, Waldo GS, et al. Domain orientation in the inactive response regulator *Mycobacterium tuberculosis* MtrA provides a barrier to activation. *Biochemistry*. 2007; 46(23):6733–43. doi: [10.1021/bi602546q](https://doi.org/10.1021/bi602546q) PMID: [17511470](https://pubmed.ncbi.nlm.nih.gov/17511470/); PubMed Central PMCID: PMC2528954.
13. King-Scott J, Nowak E, Mylonas E, Panjekar S, Roessle M, Svergun DI, et al. The structure of a full-length response regulator from *Mycobacterium tuberculosis* in a stabilized three-dimensional domain-swapped, activated state. *The Journal of biological chemistry*. 2007; 282(52):37717–29. doi: [10.1074/jbc.M705081200](https://doi.org/10.1074/jbc.M705081200) PMID: [17942407](https://pubmed.ncbi.nlm.nih.gov/17942407/).
14. Robinson VL, Wu T, Stock AM. Structural analysis of the domain interface in DrrB, a response regulator of the OmpR/PhoB subfamily. *Journal of bacteriology*. 2003; 185(14):4186–94. PMID: [12837793](https://pubmed.ncbi.nlm.nih.gov/12837793/); PubMed Central PMCID: PMC164896.
15. Nowak E, Panjekar S, Konarev P, Svergun DI, Tucker PA. The structural basis of signal transduction for the response regulator PrrA from *Mycobacterium tuberculosis*. *The Journal of biological chemistry*. 2006; 281(14):9659–66. doi: [10.1074/jbc.M512004200](https://doi.org/10.1074/jbc.M512004200) PMID: [16434396](https://pubmed.ncbi.nlm.nih.gov/16434396/).
16. Menon S, Wang S. Structure of the response regulator PhoP from *Mycobacterium tuberculosis* reveals a dimer through the receiver domain. *Biochemistry*. 2011; 50(26):5948–57. doi: [10.1021/bi2005575](https://doi.org/10.1021/bi2005575) PMID: [21634789](https://pubmed.ncbi.nlm.nih.gov/21634789/); PubMed Central PMCID: PMC3133661.
17. Bachhawat P, Swapna GV, Montelione GT, Stock AM. Mechanism of activation for transcription factor PhoB suggested by different modes of dimerization in the inactive and active states. *Structure*. 2005; 13(9):1353–63. doi: [10.1016/j.str.2005.06.006](https://doi.org/10.1016/j.str.2005.06.006) PMID: [16154092](https://pubmed.ncbi.nlm.nih.gov/16154092/); PubMed Central PMCID: PMC3685586.
18. Needham JV, Chen TY, Falke JJ. Novel ion specificity of a carboxylate cluster Mg(II) binding site: strong charge selectivity and weak size selectivity. *Biochemistry*. 1993; 32(13):3363–7. PMID: [8461299](https://pubmed.ncbi.nlm.nih.gov/8461299/).
19. Bachhawat P, Stock AM. Crystal structures of the receiver domain of the response regulator PhoP from *Escherichia coli* in the absence and presence of the phosphoryl analog beryllifluoride. *Journal of bacteriology*. 2007; 189(16):5987–95. doi: [10.1128/JB.00049-07](https://doi.org/10.1128/JB.00049-07) PMID: [17545283](https://pubmed.ncbi.nlm.nih.gov/17545283/); PubMed Central PMCID: PMC1952025.
20. Cerutti DS, Le Trong I, Stenkamp RE, Lybrand TP. Simulations of a protein crystal: explicit treatment of crystallization conditions links theory and experiment in the streptavidin-biotin complex. *Biochemistry*. 2008; 47(46):12065–77. doi: [10.1021/bi800894u](https://doi.org/10.1021/bi800894u) PMID: [18950193](https://pubmed.ncbi.nlm.nih.gov/18950193/); PubMed Central PMCID: PMC2765329.
21. Banerjee R, Yan H, Cukier RI. Conformational transition of response regulator RR468 in a two-component system signal transduction process. *J Phys Chem B*. 2014; 118(18):4727–42. doi: [10.1021/jp4122968](https://doi.org/10.1021/jp4122968) PMID: [24731214](https://pubmed.ncbi.nlm.nih.gov/24731214/).
22. Knaggs MH, Salsbury FR Jr., Edgell MH, Fetrow JS. Insights into correlated motions and long-range interactions in CheY derived from molecular dynamics simulations. *Biophys J*. 2007; 92(6):2062–79. doi: [10.1529/biophysj.106.081950](https://doi.org/10.1529/biophysj.106.081950) PMID: [17172298](https://pubmed.ncbi.nlm.nih.gov/17172298/); PubMed Central PMCID: PMC1861790.
23. Pioszak AA, Ninfa AJ. Mutations altering the N-terminal receiver domain of NRI (NtrC) That prevent dephosphorylation by the NRII-PII complex in *Escherichia coli*. *Journal of bacteriology*. 2004; 186(17): 5730–40. doi: [10.1128/JB.186.17.5730-5740.2004](https://doi.org/10.1128/JB.186.17.5730-5740.2004) PMID: [15317778](https://pubmed.ncbi.nlm.nih.gov/15317778/); PubMed Central PMCID: PMC516846.
24. Zheng W, Brooks B. Identification of dynamical correlations within the myosin motor domain by the normal mode analysis of an elastic network model. *Journal of molecular biology*. 2005; 346(3):745–59. PMID: [15713460](https://pubmed.ncbi.nlm.nih.gov/15713460/).

25. Zheng W, Brooks BR, Doniach S, Thirumalai D. Network of dynamically important residues in the open/closed transition in polymerases is strongly conserved. *Structure*. 2005; 13(4):565–77. doi: [10.1016/j.str.2005.01.017](https://doi.org/10.1016/j.str.2005.01.017) PMID: [15837195](https://pubmed.ncbi.nlm.nih.gov/15837195/).
26. Zheng W, Brooks BR, Hummer G. Protein conformational transitions explored by mixed elastic network models. *Proteins*. 2007; 69(1):43–57. doi: [10.1002/prot.21465](https://doi.org/10.1002/prot.21465) PMID: [17596847](https://pubmed.ncbi.nlm.nih.gov/17596847/).
27. Grant BJ, Rodrigues AP, ElSawy KM, McCammon JA, Caves LS. Bio3d: an R package for the comparative analysis of protein structures. *Bioinformatics*. 2006; 22(21):2695–6. doi: [10.1093/bioinformatics/btl461](https://doi.org/10.1093/bioinformatics/btl461) PMID: [16940322](https://pubmed.ncbi.nlm.nih.gov/16940322/).
28. Sola M, Gomis-Ruth FX, Serrano L, Gonzalez A, Coll M. Three-dimensional crystal structure of the transcription factor PhoB receiver domain. *Journal of molecular biology*. 1999; 285(2):675–87. PMID: [9878437](https://pubmed.ncbi.nlm.nih.gov/9878437/).
29. Gao R, Stock AM. Molecular strategies for phosphorylation-mediated regulation of response regulator activity. *Current opinion in microbiology*. 2010; 13(2):160–7. doi: [10.1016/j.mib.2009.12.009](https://doi.org/10.1016/j.mib.2009.12.009) PMID: [20080056](https://pubmed.ncbi.nlm.nih.gov/20080056/); PubMed Central PMCID: [PMC2859964](https://pubmed.ncbi.nlm.nih.gov/PMC2859964/).
30. Kern D, Volkman BF, Luginbuhl P, Nohaile MJ, Kustu S, Wemmer DE. Structure of a transiently phosphorylated switch in bacterial signal transduction. *Nature*. 1999; 402(6764):894–8. doi: [10.1038/47273](https://doi.org/10.1038/47273) PMID: [10622255](https://pubmed.ncbi.nlm.nih.gov/10622255/).
31. Birck C, Mourey L, Gouet P, Fabry B, Schumacher J, Rousseau P, et al. Conformational changes induced by phosphorylation of the FixJ receiver domain. *Structure*. 1999; 7(12):1505–15. PMID: [10647181](https://pubmed.ncbi.nlm.nih.gov/10647181/).
32. Park S, Meyer M, Jones AD, Yennawar HP, Yennawar NH, Nixon BT. Two-component signaling in the AAA + ATPase DctD: binding Mg²⁺ and BeF₃⁻ selects between alternate dimeric states of the receiver domain. *FASEB journal: official publication of the Federation of American Societies for Experimental Biology*. 2002; 16(14):1964–6. doi: [10.1096/fj.02-0395fje](https://doi.org/10.1096/fj.02-0395fje) PMID: [12368235](https://pubmed.ncbi.nlm.nih.gov/12368235/).
33. Gardino AK, Volkman BF, Cho HS, Lee SY, Wemmer DE, Kern D. The NMR solution structure of BeF₃⁻-activated Spo0F reveals the conformational switch in a phosphorelay system. *Journal of molecular biology*. 2003; 331(1):245–54. PMID: [12875849](https://pubmed.ncbi.nlm.nih.gov/12875849/).
34. Lee SY, Cho HS, Pelton JG, Yan D, Berry EA, Wemmer DE. Crystal structure of activated CheY. Comparison with other activated receiver domains. *The Journal of biological chemistry*. 2001; 276(19):16425–31. doi: [10.1074/jbc.M101002200](https://doi.org/10.1074/jbc.M101002200) PMID: [11279165](https://pubmed.ncbi.nlm.nih.gov/11279165/).
35. Bellsollell L, Prieto J, Serrano L, Coll M. Magnesium binding to the bacterial chemotaxis protein CheY results in large conformational changes involving its functional surface. *Journal of molecular biology*. 1994; 238(4):489–95. doi: [10.1006/jmbi.1994.1308](https://doi.org/10.1006/jmbi.1994.1308) PMID: [8176739](https://pubmed.ncbi.nlm.nih.gov/8176739/).
36. Feher VA, Cavanagh J. Millisecond-timescale motions contribute to the function of the bacterial response regulator protein Spo0F. *Nature*. 1999; 400(6741):289–93. doi: [10.1038/22357](https://doi.org/10.1038/22357) PMID: [10421374](https://pubmed.ncbi.nlm.nih.gov/10421374/).
37. Bobay BG, Hoch JA, Cavanagh J. Dynamics and activation in response regulators: the beta4-alpha4 loop. *Biomolecular concepts*. 2012; 3(2):175–82. doi: [10.1515/bmc-2011-0063](https://doi.org/10.1515/bmc-2011-0063) PMID: [24494032](https://pubmed.ncbi.nlm.nih.gov/24494032/); PubMed Central PMCID: [PMC3909562](https://pubmed.ncbi.nlm.nih.gov/PMC3909562/).
38. Stephenson SJ, Perego M. Interaction surface of the Spo0A response regulator with the Spo0E phosphatase. *Molecular microbiology*. 2002; 44(6):1455–67. PMID: [12067336](https://pubmed.ncbi.nlm.nih.gov/12067336/).
39. Bent CJ, Isaacs NW, Mitchell TJ, Riboldi-Tunnicliffe A. Crystal structure of the response regulator O2 receiver domain, the essential YycF two-component system of *Streptococcus pneumoniae* in both complexed and native states. *Journal of bacteriology*. 2004; 186(9):2872–9. PMID: [15090529](https://pubmed.ncbi.nlm.nih.gov/15090529/); PubMed Central PMCID: [PMC387779](https://pubmed.ncbi.nlm.nih.gov/PMC387779/).
40. Toro-Roman A, Wu T, Stock AM. A common dimerization interface in bacterial response regulators KdpE and TorR. *Protein science: a publication of the Protein Society*. 2005; 14(12):3077–88. doi: [10.1110/ps.051722805](https://doi.org/10.1110/ps.051722805) PMID: [16322582](https://pubmed.ncbi.nlm.nih.gov/16322582/); PubMed Central PMCID: [PMC2253231](https://pubmed.ncbi.nlm.nih.gov/PMC2253231/).
41. Hickey JM, Lovell S, Battaile KP, Hu L, Middaugh CR, Hefty PS. The atypical response regulator protein ChxR has structural characteristics and dimer interface interactions that are unique within the OmpR/PhoB subfamily. *The Journal of biological chemistry*. 2011; 286(37):32606–16. doi: [10.1074/jbc.M111.220574](https://doi.org/10.1074/jbc.M111.220574) PMID: [21775428](https://pubmed.ncbi.nlm.nih.gov/21775428/); PubMed Central PMCID: [PMC3173177](https://pubmed.ncbi.nlm.nih.gov/PMC3173177/).
42. Morcos F, Pagnani A, Lunt B, Bertolino A, Marks DS, Sander C, et al. Direct-coupling analysis of residue coevolution captures native contacts across many protein families. *Proceedings of the National Academy of Sciences of the United States of America*. 2011; 108(49):E1293–301. doi: [10.1073/pnas.1111471108](https://doi.org/10.1073/pnas.1111471108) PMID: [22106262](https://pubmed.ncbi.nlm.nih.gov/22106262/); PubMed Central PMCID: [PMC3241805](https://pubmed.ncbi.nlm.nih.gov/PMC3241805/).
43. Jones DT, Buchan DW, Cozzetto D, Pontil M. PSICOV: precise structural contact prediction using sparse inverse covariance estimation on large multiple sequence alignments. *Bioinformatics*. 2012; 28(2):184–90. doi: [10.1093/bioinformatics/btr638](https://doi.org/10.1093/bioinformatics/btr638) PMID: [22101153](https://pubmed.ncbi.nlm.nih.gov/22101153/).

44. Kamisetty H, Ovchinnikov S, Baker D. Assessing the utility of coevolution-based residue-residue contact predictions in a sequence- and structure-rich era. *Proceedings of the National Academy of Sciences of the United States of America*. 2013; 110(39):15674–9. doi: [10.1073/pnas.1314045110](https://doi.org/10.1073/pnas.1314045110) PMID: [24009338](https://pubmed.ncbi.nlm.nih.gov/24009338/); PubMed Central PMCID: PMC3785744.
45. Wang C, Sang J, Wang J, Su M, Downey JS, Wu Q, et al. Mechanistic insights revealed by the crystal structure of a histidine kinase with signal transducer and sensor domains. *PLoS biology*. 2013; 11(2): e1001493. doi: [10.1371/journal.pbio.1001493](https://doi.org/10.1371/journal.pbio.1001493) PMID: [23468592](https://pubmed.ncbi.nlm.nih.gov/23468592/); PubMed Central PMCID: PMC3582566.
46. Dago AE, Schug A, Procaccini A, Hoch JA, Weigt M, Szurmant H. Structural basis of histidine kinase autophosphorylation deduced by integrating genomics, molecular dynamics, and mutagenesis. *Proceedings of the National Academy of Sciences of the United States of America*. 2012; 109(26): E1733–42. doi: [10.1073/pnas.1201301109](https://doi.org/10.1073/pnas.1201301109) PMID: [22670053](https://pubmed.ncbi.nlm.nih.gov/22670053/); PubMed Central PMCID: PMC3387055.
47. McDonald LR, Whitley MJ, Boyer JA, Lee AL. Colocalization of fast and slow timescale dynamics in the allosteric signaling protein CheY. *Journal of molecular biology*. 2013; 425(13):2372–81. doi: [10.1016/j.jmb.2013.04.029](https://doi.org/10.1016/j.jmb.2013.04.029) PMID: [23648838](https://pubmed.ncbi.nlm.nih.gov/23648838/); PubMed Central PMCID: PMC3703654.
48. Jeong KW, Ko H, Lee SA, Hong E, Ko S, Cho HS, et al. Backbone dynamics of an atypical orphan response regulator protein, *Helicobacter pylori* 1043. *Molecules and cells*. 2013; 35(2):158–65. doi: [10.1007/s10059-013-2303-z](https://doi.org/10.1007/s10059-013-2303-z) PMID: [23456337](https://pubmed.ncbi.nlm.nih.gov/23456337/); PubMed Central PMCID: PMC3887898.
49. Gao R, Tao Y, Stock AM. System-level mapping of *Escherichia coli* response regulator dimerization with FRET hybrids. *Molecular microbiology*. 2008; 69(6):1358–72. doi: [10.1111/j.1365-2958.2008.06355.x](https://doi.org/10.1111/j.1365-2958.2008.06355.x) PMID: [18631241](https://pubmed.ncbi.nlm.nih.gov/18631241/); PubMed Central PMCID: PMC2586830.
50. Mack TR, Gao R, Stock AM. Probing the roles of the two different dimers mediated by the receiver domain of the response regulator PhoB. *Journal of molecular biology*. 2009; 389(2):349–64. doi: [10.1016/j.jmb.2009.04.014](https://doi.org/10.1016/j.jmb.2009.04.014) PMID: [19371748](https://pubmed.ncbi.nlm.nih.gov/19371748/); PubMed Central PMCID: PMC2716121.
51. Remmert M, Biegert A, Hauser A, Soding J. HHblits: lightning-fast iterative protein sequence searching by HMM-HMM alignment. *Nat Methods*. 2012; 9(2):173–5. doi: [10.1038/nmeth.1818](https://doi.org/10.1038/nmeth.1818) PMID: [22198341](https://pubmed.ncbi.nlm.nih.gov/22198341/).
52. Dunn SD, Wahl LM, Gloor GB. Mutual information without the influence of phylogeny or entropy dramatically improves residue contact prediction. *Bioinformatics*. 2008; 24(3):333–40. doi: [10.1093/bioinformatics/btm604](https://doi.org/10.1093/bioinformatics/btm604) PMID: [18057019](https://pubmed.ncbi.nlm.nih.gov/18057019/).
53. Balakrishnan S, Kamisetty H, Carbonell JG, Lee SI, Langmead CJ. Learning generative models for protein fold families. *Proteins*. 2011; 79(4):1061–78. doi: [10.1002/prot.22934](https://doi.org/10.1002/prot.22934) PMID: [21268112](https://pubmed.ncbi.nlm.nih.gov/21268112/).
54. Phillips JC, Braun R, Wang W, Gumbart J, Tajkhorshid E, Villa E, et al. Scalable molecular dynamics with NAMD. *J Comput Chem*. 2005; 26(16):1781–802. doi: [10.1002/jcc.20289](https://doi.org/10.1002/jcc.20289) PMID: [16222654](https://pubmed.ncbi.nlm.nih.gov/16222654/); PubMed Central PMCID: PMC2486339.
55. Mackerell AD Jr., Feig M, Brooks CL 3rd. Extending the treatment of backbone energetics in protein force fields: limitations of gas-phase quantum mechanics in reproducing protein conformational distributions in molecular dynamics simulations. *J Comput Chem*. 2004; 25(11):1400–15. doi: [10.1002/jcc.20065](https://doi.org/10.1002/jcc.20065) PMID: [15185334](https://pubmed.ncbi.nlm.nih.gov/15185334/).
56. Laskowski RA, Swindells MB. LigPlot+: multiple ligand-protein interaction diagrams for drug discovery. *J Chem Inf Model*. 2011; 51(10):2778–86. PMID: [21919503](https://pubmed.ncbi.nlm.nih.gov/21919503/).
57. Webb B, Sali A. Comparative Protein Structure Modeling Using MODELLER. *Curr Protoc Bioinformatics*. 2014; 47:5 6 1–5 6 32. doi: [10.1002/0471250953.bi0506s47](https://doi.org/10.1002/0471250953.bi0506s47) PMID: [25199792](https://pubmed.ncbi.nlm.nih.gov/25199792/).
58. Tama F, Brooks CL. Symmetry, form, and shape: guiding principles for robustness in macromolecular machines. *Annu Rev Biophys Biomol Struct*. 2006; 35:115–33. doi: [10.1146/annurev.biophys.35.040405.102010](https://doi.org/10.1146/annurev.biophys.35.040405.102010) PMID: [16689630](https://pubmed.ncbi.nlm.nih.gov/16689630/).
59. Best RB, Chen YG, Hummer G. Slow protein conformational dynamics from multiple experimental structures: the helix/sheet transition of arc repressor. *Structure*. 2005; 13(12):1755–63. doi: [10.1016/j.str.2005.08.009](https://doi.org/10.1016/j.str.2005.08.009) PMID: [16338404](https://pubmed.ncbi.nlm.nih.gov/16338404/).